JOURNAL OF VIROLOGY, July 2007, p. 7476–7490 Vol. 81, No. 14
0022-538X/07/$08.00+0 doi:10.1128/JVI.00308-07

Productive Human Immunodeficiency Virus Type 1 Assembly Takes Place at the Plasma Membrane▽

Andrés Finzi,[1] Alexandre Orthwein,[1] Johanne Mercier,[1] and Éric A. Cohen[1,2]*

Laboratory of Human Retrovirology, Institut de Recherches Cliniques de Montréal,[1] and Department of Microbiology and Immunology, Université de Montréal,[2] Montreal, Quebec, Canada

Received 12 February 2007/Accepted 3 May 2007

Gag proteins are necessary and sufficient to direct human immunodeficiency virus type 1 (HIV-1) particle assembly and budding. Recent evidence suggests that Gag targeting to late endosomal/multivesicular body (LE/MVB) compartments occurs prior to viral particle budding at the plasma membrane (PM). However, the route that Gag follows before reaching its steady-state destinations still remains a subject of debate. Using a subcellular fractionation method that separates PM from LE/MVB combined with pulse-chase labeling, we analyzed Gag trafficking in HIV-1-producing HEK 293T cells. Our results reveal that the majority of newly synthesized Gag is primarily targeted to the PM. While PM-targeted Gag was efficiently released, a significant fraction of the remaining cell surface-associated Gag was found to be subsequently internalized to LE/MVB, where it accumulated, thus accounting for the majority of LE/MVB-associated Gag. Importantly, this accumulation of Gag in LE/MVB was found to be cholesterol dependent since it was sensitive to the sterol-binding drugs filipin and methyl-β-cyclodextrin. These results point towards the PM as being the primary site of productive HIV-1 assembly in cells that also support Gag accumulation in intracellular compartments.

Production of human immunodeficiency virus type 1 (HIV-1) particles involves a series of coordinated events that includes targeting of viral structural proteins at a membrane assembly site, incorporation of the RNA genome, clustering of Gag/Gag-Pol molecules, and subsequent release of immature virions, which undergo a protease-mediated maturation process to become fully infectious. While the envelope glycoproteins (Env) and the *pol*-encoded enzymes (protease, reverse transcriptase, and integrase) are required for the production of infectious particles, expression of Gag polyprotein ($Pr55^{gag}$) alone is necessary and sufficient for the assembly and release of noninfectious virus-like particles (18). $Pr55^{gag}$ is constituted of four structural components that are cleaved by the viral protease concomitant to the budding process, to generate the mature virion-associated Gag products matrix (MA or p17), capsid (CA or p24), nucleocapsid (NC or p7), and p6, as well as two spacer peptides, SP1 and SP2 (for a review, see references 16 and 18). Three functional domains (M, I, and L) within Gag capable of mediating the formation and release of virus-like particles have been identified (for a review, see references 16 and 18). M, the membrane-binding domain, which consists of an N-terminal myristylic acid group and a highly basic domain in MA, allows the precursor to associate with a membrane assembly and budding site following its synthesis on cytosolic polysomes. I, the interaction domain, promotes Gag-Gag multimerization and consists of the region spanning the C-terminus domain of CA and the N-terminus domain of NC. L, the late domain, is responsible for the pinching-off of nascent particles from cellular membranes during the release step. The L domain through its highly conserved PTAP and YPLTSL late motifs located in p6 recruits Tsg101, AIP1, and other components of the endosomal sorting complex required for transport, which are normally responsible for directing the formation of intralumenal vesicles within multivesicular bodies (MVB) (for a review, see references 4 and 33).

HIV-1 Gag precursors have long been considered to assemble and bud from the plasma membrane (PM) in T lymphocytes as well as in most transformed cell lines, such as HEK 293T, HeLa, and T-cell lines (9, 33). However, recent reports have challenged this notion mainly because in these cells, a significant proportion of Gag was also found to localize to intracellular compartments that express late endosome (LE) or MVB markers (12, 21, 46, 54). Furthermore, this internal localization of Gag was particularly pronounced in macrophages, where very large numbers of viral particles are found to accumulate within LE/MVB compartments (36, 42, 45, 48). However, the molecular mechanisms that control cell surface versus LE/MVB accumulation of $Pr55^{gag}$ and, consequently, the choice of the viral assembly and budding site are still poorly understood. One key specific aspect that remains to be clarified is the route that $Pr55^{gag}$ follows to reach its PM or LE/MVB steady-state location. Interestingly, two models are emerging from recent studies to explain this dual-steady-state Gag localization in different cell types. One model proposes that $Pr55^{gag}$ is first inserted into endosomal membranes and then, depending on how the process of LE/MVB-mediated exocytosis is regulated in specific cell types, either retained (macrophages) or further transported to the PM (e.g., T lymphocytes, HeLa, and HEK 293T cells) (12, 21, 30, 39, 45, 46, 48, 49, 54). In this model, LE/MVB compartments represent early intermediates where assembly and budding can take place. In contrast, the other model postulates that newly synthesized $Pr55^{gag}$ is first targeted to the PM, where viral assembly and release occur; nonreleased Gag products are subsequently internalized to-

* Corresponding author. Mailing address: Laboratory of Human Retrovirology, Institut de Recherches Cliniques de Montréal (IRCM), 110, Avenue des Pins Ouest, Montreal, Quebec, Canada H2W 1R7. Phone: (514) 987-5804. Fax: (514) 987-5691. E-mail: eric.cohen@ircm.qc.ca.

▽ Published ahead of print on 16 May 2007.

wards LE/MVB (22, 24, 34, 51) in a process that is sensitive to endocytosis inhibitors (24, 34).

To distinguish between these two models, we adapted a subcellular fractionation method that efficiently separates the PM from LE/MVB. This method coupled to pulse-chase labeling and immunoprecipitation analysis allowed a dynamic and quantitative monitoring of newly synthesized Gag trafficking in HIV-1 provirus-transfected HEK 293T cells. Our results reveal that the majority of newly synthesized $Pr55^{gag}$ is targeted to the PM. Importantly, however, a significant fraction of PM-associated Gag products was found to be internalized over time to LE/MVB by means of endocytosis. This process was not affected by chlorpromazine, an inhibitor of clathrin-dependent endocytosis, but it was efficiently blocked by filipin and methyl-β-cyclodextrin (MβCD), two endocytosis inhibitors known to affect PM-associated cholesterol. Taken together, our data identify the PM as being the primary site of productive HIV-1 assembly and release in cells that also support Gag accumulation into intracellular compartments.

MATERIALS AND METHODS

Cells and plasmids. HEK 293T cells were maintained as described previously (28). The HIV-1 molecular clone HxBc2 (27), the bicistronic pBud-DR construct (14), and the SVCMV CD4 expression plasmid (28) were previously described. The HxBc2 PR^- Env^- provirus was constructed by replacing the SalI/BamHI fragment of HxBc2 PR^- (19) with the SalI/BamHI fragment of HxBc2 Env^- (7).

Abs. The following antibodies (Abs) were used. L243 (immunoglobulin G2a [IgG2a]), a mouse monoclonal Ab that binds a specific HLA-DRα conformational determinant dependent on the correct conformation of the α/β heterodimer (44), mouse monoclonal anti-HLA-DR β-chain XD5 Ab (47), anti-CD4 (OKT4) (catalog no. CRL-8002), and anti-p24 (catalog no. HB-9725) monoclonal Abs were isolated from supernatants of cultured hybridoma cells obtained from the American Type Culture Collection (Manassas, VA). Rabbit anti-p24 polyclonal Ab (catalog no. 4250) was from the NIH AIDS Reference and Reagent Program. Mouse anti-Lamp1 (H5G11, IgG1) was from Santa Cruz Biotechnology, Santa Cruz, CA. Mouse anti-CD63 (H5C6, IgG1) was from the Hybridoma Bank, NICHD, University of Iowa. Anti-Na^+-K^+ ATPase (M7-PB-E9) and anti-α-tubulin (T5168) were from Sigma-Aldrich, Oakville, Ontario, Canada. Alexa-594-conjugated anti-mouse IgG was from Molecular Probes, Burlington, Ontario, Canada.

Transfections and metabolic labeling. Transfections were performed as described previously (61); experiments were done 48 h posttransfection. For pulse-chase experiments, transfectants were metabolically labeled with 1 mCi/ml [^{35}S]methionine-cysteine (^{35}S protein-labeling mix; Perkin-Elmer, Wellesley, MA) in Dulbecco's modified Eagle's medium (DMEM) lacking methionine and cysteine and supplemented with 5% dialyzed fetal bovine serum for 10 min and chased for different time intervals in DMEM containing excess unlabeled methionine and cysteine. When indicated, chlorpromazine (10 μg/ml), filipin (4 μg/ml), MβCD (8 mM), or nocodazole (10 μg/ml) was added during the starvation period (30 min) and maintained throughout the chase. All drugs were purchased from Sigma-Aldrich.

Subcellular fractionation, immunoprecipitation, enzymatic assay, and Western blotting. Subcellular fractionation was performed as described previously (53). Briefly, 5 million HEK 293T cells were harvested in 250 μl of homogenization buffer (0.25 M sucrose, 78 mM KCl, 4 mM $MgCl_2$, 8.4 mM $CaCl_2$, 10 mM EGTA, and 50 mM HEPES-NaOH [pH 7.0], containing a cocktail of protease inhibitors [Roche, Mississauga, Ontario, Canada]) and lysed for 60 s using a pellet pestle with a cordless motor (Kontes, Vineland, NJ). Homogenates were centrifuged at 1,000 × *g* for 5 min to pellet nuclei and any cell debris. Postnuclear supernatant (PNS) was loaded onto a 5 to 20% linear Optiprep gradient according to the manufacturer's instructions (application sheet S23; Axis-Shield, Norton, MA) and spun at 150,000 × *g* at 4°C for 20 h using an SW41 ultracentrifuge rotor (Beckman, Mississauga, Ontario, Canada). Fourteen fractions (800 μl) were collected from the top of the gradient and lysed with 200 μl of 5× deoxycholate-containing radioimmunoprecipitation assay buffer (RIPA.DOC: 700 mM NaCl, 40 mM Na_2HPO_4, 10 mM NaH_2PO4, 5% NP-40, 2.5% sodium deoxycholate, 0.25% sodium dodecyl sulfate [SDS]) containing a cocktail of protease inhibitors. Immunoprecipitations were performed on each fraction as follows. Fractions were precleared with the corresponding normal serum for 2 h at 4°C before being immunoprecipitated for 3 h at 4°C with a monoclonal anti-p24 Ab or a polyclonal anti-p24 serum as described previously (61). For denaturing conditions, each fraction was denatured as described previously (41) before immunoprecipitation with a polyclonal anti-p24 serum. Analysis of released viral particles was performed on tissue culture supernatants that were cleared by low-speed centrifugation (10 min at 400 × *g*) and passed through a 0.45-μm-pore-size filter (Costar, Cambridge, MA). Viral particles were pelleted from the filtrate by ultracentrifugation through a 20% (wt/vol) sucrose cushion in phosphate-buffered saline (PBS) for 120 min at 130,000 × *g* at 4°C, lysed in 1× RIPA.DOC buffer containing a cocktail of protease inhibitors, and immunoprecipitated as described above. Immunocomplexes were separated by SDS-polyacrylamide gel electrophoresis and analyzed by autoradiography. Quantitation of radioactive Gag-related bands in each fraction was performed using a PhosphorImager equipped with the ImageQuant software 5.0.

Enzymatic assays performed to identify alkaline phosphatase-containing fractions were performed as follows. Twenty-five microliters of each fraction was mixed with 15 μl of 4 mM 4-methylumbelliferyl phosphate (Sigma-Aldrich) dissolved in a citrate buffer (50 mM citric acid, 70 mM Na_2HPO_4 [pH 4.5]). After 2 h of incubation at 37°C, the reaction was stopped by using 50 μl of glycine buffer (100 mM glycine [pH 10.4], 10 mM EDTA, 2% Triton X-100). Samples were excited at 355 nm and read at 460 nm on a multiple reader (Wallac Victor, Wallac Oy, Turku, Finland). Finally, the presence of Na^+-K^+ ATPase, CD63, and Lamp1 in each fraction was determined by Western blotting as previously described (28). For HLA-DR detection, each fraction was immunoprecipitated with the L243 conformational Ab before being detected by Western blotting using the anti-HLA-DR β-chain XD5 Ab.

Cell surface biotinylation, biotinylated Tfr, and cell surface CD4. Forty-eight hours posttransfection, cells were washed three times with ice-cold PBS and then labeled in PBS containing 480 μg/ml of sulfo-NHS-SS-biotin (Pierce, Rockford, IL) for 30 min at 0°C. Cells were then washed with cold PBS-Tris (50 mM) to quench the remaining biotinylation reagent. For biotinylated transferrin (Tfr), cells were incubated for 15 min at 0°C with human biotin-Tfr (25 μg/ml) (Sigma-Aldrich). Cells were then washed twice with cold PBS. For both experiments, cells were then mechanically lysed as described above and the PNS was subjected to subcellular fractionation. Of note, due to the high density of fractions 10 to 14, we could not perform dot blot analysis for cell surface biotinylation. Therefore, biotinylated cell surface proteins were loaded on SDS-polyacrylamide gel electrophoresis gel (12.5%) and allowed to enter the gel by a short migration. Fractions were subsequently analyzed by Western blotting using a streptavidin-horseradish peroxidase conjugate (Amersham, Baie d'Urfe, Quebec, Canada). For the analysis of cell surface biotinylation in drug-treated cells, drugs were added for 30 min at 37°C in DMEM before subjecting cells to the procedure described above (drugs were present throughout the experiment). For cell surface CD4 analysis, HEK 293T cells were cotransfected with the HxBc2 proviral construct and SVCMV CD4, a plasmid encoding CD4. Forty-eight hours later, cells were washed with ice-cold PBS and then labeled with anti-CD4 (OKT4) Ab resuspended in PBS for 30 min at 0°C to mark cell surface CD4. Cells were washed twice with cold PBS prior to mechanical lysis and fractionation as previously described. Cell surface-bound OKT4 was revealed by Western blotting using a goat anti-mouse Ab coupled to peroxidase (Amersham), as described previously (28).

EM. For electron microscopy (EM), after subcellular fractionation, fractions 2 and 3, 6 and 7, and 13 and 14 were fixed for 1 h at 4°C with 2.5% glutaraldehyde–0.1 M cacodylate (pH 7.3). Fixed fractions were subsequently precipitated for 15 min at 40,000 × *g* in an F-20/microrotor (Sorvall, Burlington, Ontario, Canada). Fraction pellets were washed three times with 0.1 M cacodylate (pH 7.3) before incubation in 1% OsO_4 in cacodylate buffer for 45 min at 21°C. Pellets were dehydrated in alcohol series before embedding and polymerization in Durcupan resin (Sigma-Aldrich). Thin sectioning was done with an ultramicrotome system (Reichert-Jung Ultracut E; Reichert-Jung, Rochester, NY), and the sections were placed on nickel 200mESH grids (Canemco, Lakefield, Quebec, Canada). Cells were stained with 1% uranyl acetate in 70% ethanol and lead citrate. For immunogold staining, samples were processed as described previously (32). Polyclonal anti-p24 Ab staining was followed by incubation with a goat anti-rabbit serum coupled to 12- or 18-nm gold beads (Jackson Laboratories, Bar Harbor, ME). The grids were examined on a JEOL JEM-1200 EX transmission electron microscope.

Cholera toxin and Tfr uptake. Cells were treated for 30 min with chlorpromazine (10 μg/ml), filipin (4 μg/ml), or MβCD (8 mM) at 37°C (drugs maintained throughout the experiment), subsequently washed with PBS, and incubated for 30 min at 0°C with either Tfr– or cholera toxin β subunit (ChTxβ)–Alexa-488 conjugates (Molecular Probes, Burlington, Ontario, Canada) in PBS. Cells were

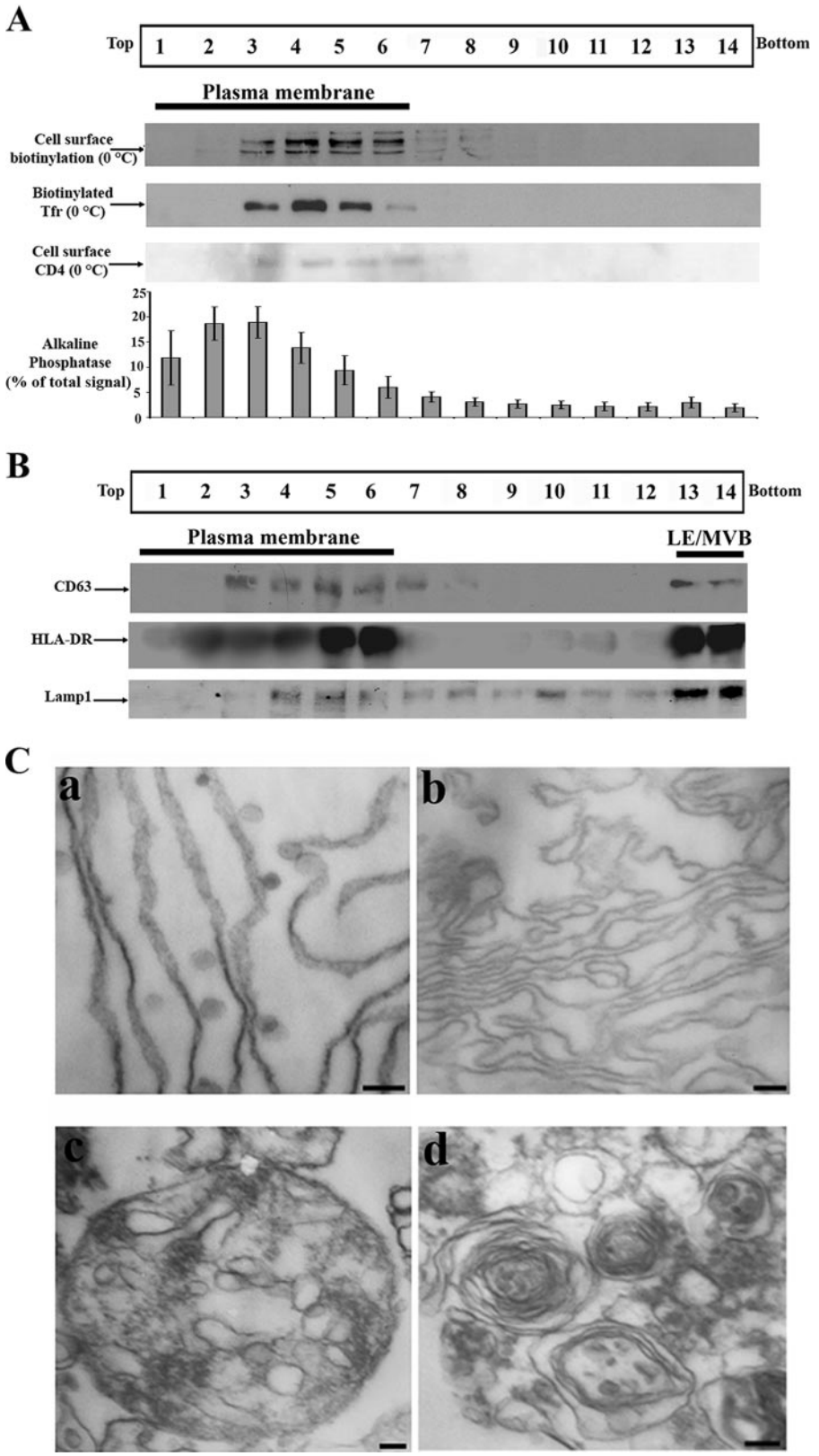

FIG. 1. PM separation from LE/MVB after iodixanol gradient-based subcellular fractionation. HEK 293T cells were transfected with the HxBc2 provirus and mechanically homogenized 48 h later. PNS production and subcellular fractionation were performed as described in Materials and Methods. (A) Plasma membrane location in the gradient. Cells were cell surface biotinylated or incubated with biotinylated Tfr at 0°C. Alternatively cells were cotransfected with a CD4 expressor and cell surface CD4 was labeled with an anti-CD4 Ab at 0°C; detection of the CD4-bound Ab was performed by Western blotting as indicated in Materials and Methods. Biotinylated cell surface proteins and biotinylated Tfr

then washed with cold PBS and then incubated at 37°C for 10 min to allow Tfr or ChTxβ internalization. Cytospin, paraformaldehyde fixation, staining of nuclei, and mounting were performed as previously described (14). Cells were examined by conventional epifluorescence micrographs on a Zeiss Cell Observer system (Zeiss, Toronto, Ontario, Canada) equipped with an Axiovert 200 M microscope and a Zeiss Axiocam ultra-high-resolution monochrome digital camera, using the ×100 oil lens. Images were digitally deconvoluted with the AxioVision 4.4 software using the nearest-neighbor deconvolution method.

RESULTS

Characterization of a subcellular fractionation method that separates PM from LE/MVB. It is now well established that HIV-1 Gag localizes at steady state both at the PM and in LE/MVB in several established human cell lines, including HEK 293T cells, which have been used as model systems to study Gag trafficking as well as HIV-1 particle assembly and release (12, 14, 21, 38, 54). To gain insights into this dual Gag localization (PM versus LE/MVB), we have adapted a previously described subcellular fractionation method that was based on a 5 to 20% continuous iodixanol (Optiprep) gradient (53). Of note, all of the characterization steps described below were performed on HxBc2 provirus-transfected HEK 293T cells that were lysed mechanically in an osmotic buffer 48 h posttransfection. PNS was fractionated by iodixanol gradient after high-speed and prolonged centrifugation periods (see Materials and Methods). Fourteen fractions were collected from the top of the gradient and analyzed for the presence of different endogenous and exogenous cellular markers. In an effort to localize where PM migrated into the gradient, we biotinylated exposed cell surface-associated proteins; the majority of the biotin-labeled proteins were found in light-density fractions, identifying them as PM associated (mostly fractions 3 to 6). Similarly, biotin-conjugated Tfr was also incubated with HEK 293T cells at 0°C to label the PM and gave similar results; biotin-conjugated Tfr was exclusively found in light-density fractions (mostly fractions 3 to 6) (Fig. 1A). Furthermore, when cells were cotransfected with a CD4 expressor and incubated at 0°C to block endocytosis of the receptor bound to an anti-CD4 antibody, cell surface CD4 was also exclusively found in light-density fractions (fractions 3 to 6) (Fig. 1A). Similarly, Na^+-K^+ ATPase, a known PM marker (31), was also primarily found in light-density fractions (fractions 2 to 6 [data not shown]). Finally, an enzymatic assay was performed on each fraction to detect the presence of alkaline phosphatase, an enzyme previously shown to be PM associated (15). As expected, alkaline phosphatase activity was mainly found in light-density fractions (Fig. 1A [80% of the total enzymatic signal was associated with light-density fractions 1 to 6]). We next examined LE/MVB migration into the Optiprep gradient by Western blotting using antibodies directed against late endosomal markers. CD63 was found in high-density fractions (fractions 13 and 14) but also in PM-enriched fractions (fractions 3 to 7 [Fig. 1B]). Interestingly, as recently described by Janvier and Bonifacino (23), significant fractions of CD63 localize at the PM and traffic through the cell surface before reaching late endosomes, thus explaining the presence of CD63 in light-density fractions. We then evaluated the migration of HLA-DR, another marker that was previously shown to accumulate in LE/MVB via the PM (13). When cells were cotransfected with an HLA-DR expressor, it fractionated in high-density fractions (fractions 13 and 14) but also in light-density fractions (fractions 2 to 6) (Fig. 1B), most likely reflecting its previously described cell surface localization (13). Finally, the endosomal/lysosomal marker Lamp1 was predominantly found (48%) in high-density fractions (fractions 13 and 14) and to a lesser extent between fractions 4 and 6 (25%) (Fig. 1B), the latter likely representing its previously reported PM localization (23). Altogether, these data suggested that the majority of LE/MVB migrated to high-density fractions, whereas light-density fractions were enriched in PM.

To further obtain direct evidence that these fractions were indeed PM or LE/MVB enriched, we performed transmission EM analysis of light- and high-density fractions. Briefly, provirus-transfected HEK 293T cells were mechanically lysed 48 h posttransfection and the PNS was fractionated as described above. Fractions 2 and 3, 6 and 7, and 13 and 14 were ultracentrifuged, and the resulting pellets were processed for conventional EM. As expected, light-density fractions were highly enriched in filamentous structures reminiscent of the PM (Fig.1Ca). Interestingly, these filaments presented small (50 to 100 nm) invaginations as well as separate small vesicles that were not stained by the anti-CA antibody; these structures were similar in shape and diameter to previously described caveolae and indeed were specifically labeled with an antibody directed against caveolin-1, a key component of caveolae (1, 50, 58; data not shown). When fractions 6 and 7 were analyzed by EM, we observed again a clear enrichment of filamentous structures reminiscent of the PM (Fig.1Cb); however, in contrast to fractions 2 and 3, these structures were devoid of caveola-like structures, thus suggesting that two distinct PM subpopulations appear to be separated by the fractionation procedure. Importantly, the fact that no LE/MVB structures were observed in these fractions after extensive analysis suggested that detection of markers such as CD63, Lamp1, and HLA-DR in these fractions (Fig. 1B) probably reflected the reported association of these proteins with the PM during their trafficking. Finally, when we performed EM analysis on high-density fractions (fractions 13 and 14), we observed a clear enrichment (approximately 10-fold) of multivesicular

were analyzed in each fraction by Western blotting as described in Materials and Methods. Finally, the presence of alkaline phosphatase was evaluated by incubating each fraction with its specific substrate as described in Materials and Methods. Data shown for alkaline phosphatase represent the average ± standard deviation of more than 10 independent experiments. (B) LE/MVB marker migration was analyzed by Western blotting using specific anti-CD63 and Lamp1 Abs or by immunoprecipitation/Western blotting using HLA-DR Abs. Data shown in panels A and B are representative of at least two independent experiments. (C) Fractions 2 and 3, 6 and 7, and 13 and 14 were pooled, fixed, ultracentrifuged, and processed for conventional EM. PM structures were highly enriched in fractions 2 and 3 (a) and 6 and 7 (b). Fractions 13 and 14 were highly enriched in multivesicular bodies (c) and multilamellar structures (d). Scale bars represent 200 nm in panel a and 100 nm in panels b to d. Data shown are representative of at least two independent experiments.

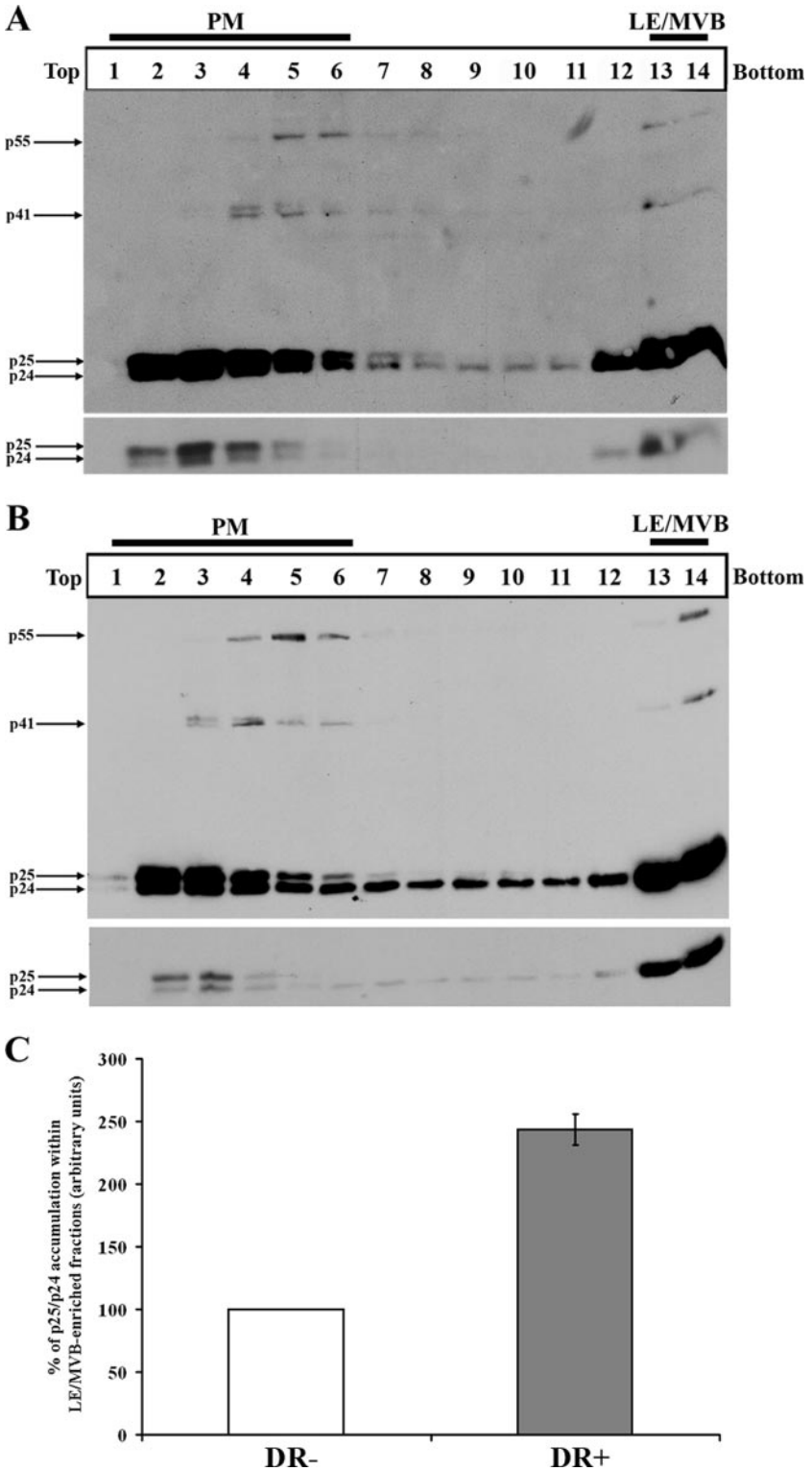

FIG. 2. HIV-1 Gag steady-state distribution after subcellular fractionation. HEK 293T cells were cotransfected with the HxBc2 provirus together with either HLA-DR or empty vector and mechanically homogenized 48 h later. PNS was processed as described in Materials and Methods. Fourteen fractions were collected from the top of the gradient, and Gag and its cleavage products were analyzed by Western blotting using a monoclonal anti-p24 Ab. (A) Steady-state Gag distribution after subcellular fractionation. (B) Steady-state distribution of Gag upon HLA-DR expression. The lower panels represent lower exposure of the mature (p25/p24) Gag products. Data shown are representative of at least two independent experiments. (C) Quantification of the relative amounts of mature Gag products (p25/p24) detected in PM- or LE/MVB-enriched fractions in the presence or absence of HLA-DR. Signals obtained for HLA-DR-negative samples were arbitrarily set to 100. Data shown are means ± standard deviations of two independent experiments.

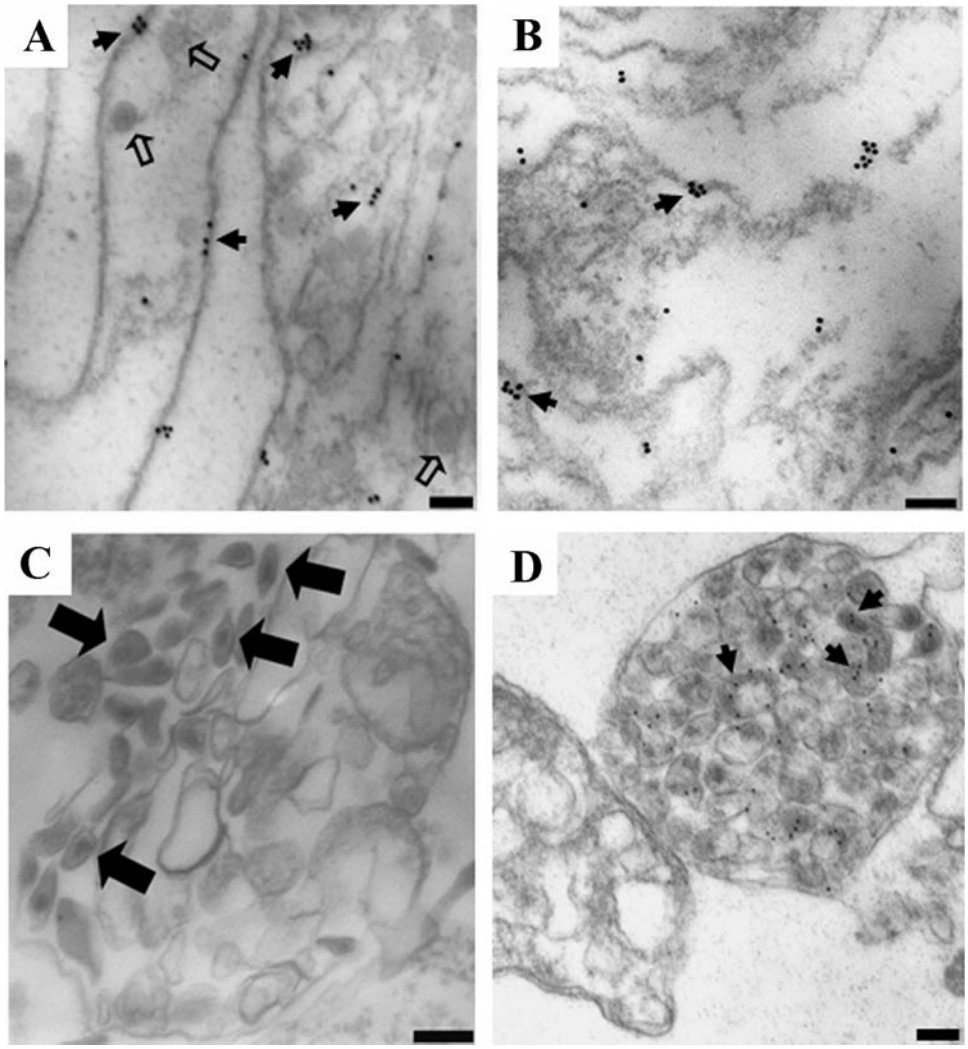

FIG. 3. Ultrastructural analysis of HIV-1 Gag association with different subcellular compartments. HEK 293T cells were transfected with the HxBc2 provirus together with an HLA-DR expressor and mechanically homogenized 48 h later. PNS production and subcellular fractionation were performed as described in Materials and Methods. Fourteen fractions were collected from the top of the gradient; fractions 2 and 3, 6 and 7, and 13 and 14 were pooled, fixed, ultracentrifuged, and observed by conventional transmission EM (C) or processed for immunogold staining with a rabbit polyclonal anti-p24 Ab followed by incubation with a goat anti-rabbit serum coupled to 18-nm (A and B) or 12-nm (D) gold beads. Filamentous structures staining positive for p24 were exclusively observed in fractions 2 and 3 (A) and 6 and 7 (B). Fractions 13 and 14 were enriched in HIV-1 particle-containing LE/MVB (C) as indicated by a positive p24 staining (D). Caveola-like structures are indicated by small open arrows. Small solid arrows indicate CA staining, whereas large solid arrows indicate mature virus. Scale bars represent 100 nm. Data shown are representative of at least two independent experiments.

(Fig.1Cc) and multilamellar (Fig.1Cd) structures. Taken together, these biochemical and electron microscopy data provide strong evidence indicating that this modified subcellular fractionation method efficiently separates PM from LE/MVB: light-density fractions were found to be enriched in PM, whereas high-density fractions were devoid of PM markers but enriched in multivesicular and multilamellar structures.

Steady-state HIV-1 Gag distribution following subcellular fractionation. Since we were able to separate PM from LE/MVB, we next addressed how HIV-1 Gag fractionated into the gradient. HEK 293T cells were transfected with an infectious molecular clone of HIV-1 (HxBc2) and fractionated 48 h later as described above. Interestingly, at steady state, two Gag populations were observed (Fig. 2A): $Pr55^{gag}$ and its cleavage products p41, p25, and p24 were primarily detected in PM-enriched fractions at the top of the gradient (mainly fractions 2 to 6), while a smaller proportion of Gag products were found in fractions enriched in LE/MVB markers at the bottom of the gradient (fractions 13 and 14). To ensure that the high-density fraction-associated Gag signal was membrane associated and indeed did not result from sedimentation of cytosolic Gag complexes, we subjected PNS from provirus-transfected HEK 293T cells to membrane permeabilization with a nonionic detergent (NP-40) known to permeabilize membrane vesicles and to solubilize membrane-associated proteins. Similar treatments were recently used to demonstrate the association of HIV-1 Gag with different cellular membranes (21, 59). As expected, after this treatment, Gag signal was absent from

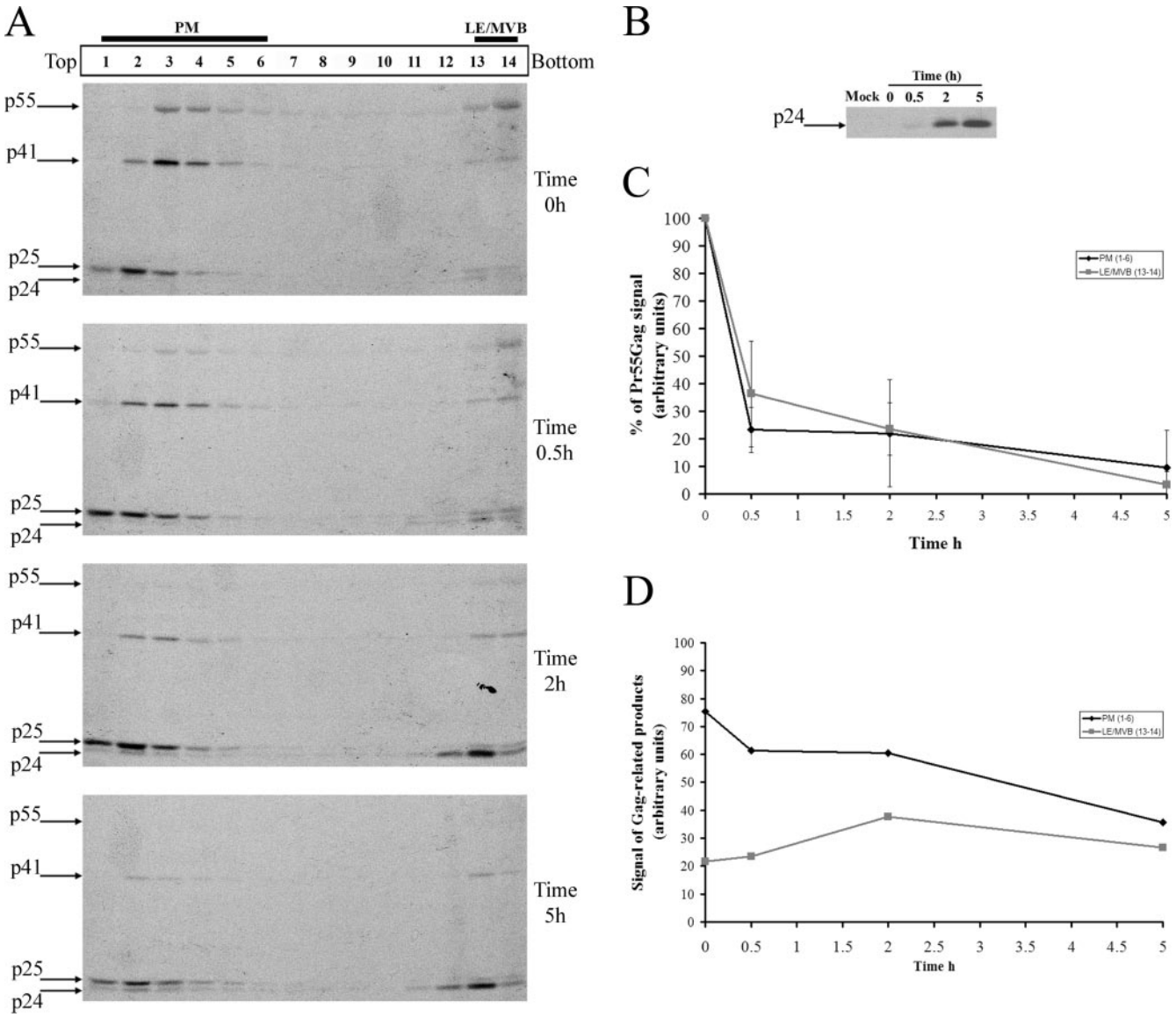

FIG. 4. Subcellular trafficking of HIV-1 Gag. (A) HEK 293T cells were transfected with the HxBc2 provirus. Two days after transfection, cells were metabolically labeled with [^{35}S]Met-Cys for 10 min and chased for various times prior to cell lysis and subcellular fractionation by Optiprep gradient centrifugation as described in Materials and Methods. Fourteen fractions were collected from the top of the gradient, and Gag-related products in each fraction were detected by immunoprecipitation using a monoclonal anti-p24 Ab. (B) Viral release during the pulse-chase analysis. Virion lysates were immunoprecipitated as for panel A. Data shown are representative of five independent experiments. (C) Quantification of the relative amounts of Pr55^{gag} in PM- and LE/MVB-enriched fractions (fractions 1 to 6 and 13 and 14, respectively) over time. Pr55^{gag} signal obtained at time zero h in PM- or LE/MVB-enriched fractions was arbitrarily set to 100. (D) Quantification of the relative amounts of Gag-related products in PM- or LE/MVB-enriched fractions over time. Quantifications were performed using ImageQuant software 5.0.

high-density fractions and was entirely detected in light-density fractions, which in addition to PM markers were associated with the cytosolic marker actin (fractions 2 to 6 [data not shown]), thus indicating that Gag located at the bottom of the gradient was detergent sensitive and as such likely to be membrane associated (data not shown).

To obtain additional evidence that LE/MVB-containing virus migrates at the bottom of the gradient, we analyzed the distribution of Gag products at steady state in the presence or absence of HLA-DR (Fig. 2) since we recently reported that HLA-DR expression in human cell lines such as HEK 293T or HeLa cells induced accumulation of Gag and HIV-1 particles in LE/MVB (14). As expected, the data of Fig. 2A and B clearly revealed a 2.5-fold increase of mature Gag product accumulation in high-density fractions in HLA-DR$^+$ as compared to HLA-DR$^-$ samples upon shorter exposure of Western blots (Fig. 2A and B, bottom panels, and C). Altogether, these results suggest that LE/MVB compartments associated with mature Gag products, normally found in virions, migrate to high-density fractions (fractions 13 and 14).

Finally, to ensure that PM or LE/MVB-associated Gag signals were not the result of cofractionation between Gag prod-

ucts and the different enriched structures, we performed immunogold staining of CA on pelleted material from fractions 2 and 3, 6 and 7, and 13 and 14 using a polyclonal anti-p24 antibody and analyzed CA staining on subcellular structures by EM. Interestingly, the filamentous structures depicted in Fig. 1C stained positive for CA (Fig. 3A). In fact, CA staining was observed on discrete patches of the PM, probably reflecting assembling structures (Fig. 3A). Similar CA staining was previously observed in pellets of purified detergent-resistant membranes isolated from Gag-expressing BSC-40 cells (11). Furthermore, analogous CA-enriched patches were also observed in fractions 6 and 7 (Fig. 3B). Finally, when high-density fractions (fractions 13 and 14) were processed for conventional EM analysis, we observed LE/MVB compartments containing structures reminiscent of fully mature viruses (Fig. 3C), in agreement with the strong accumulation of fully mature Gag (p24) detected in fractions 13 and 14 by Western blotting (Fig. 2A). Importantly, immunogold analysis of the same fractions using a polyclonal anti-p24 Ab confirmed that these structures were associated with viral particles (Fig. 3D). Of note, fractions 2 and 3, 6 and 7, and 13 and 14 isolated from mock-transfected cells remained completely unlabeled by this technique, thus indicating that CA labeling in fractions obtained from provirus-transfected cells was specific (data not shown).

Subcellular trafficking of HIV-1 Gag. To analyze the movement of newly synthesized $Pr55^{gag}$ and its cleavage products between the PM and LE/MVB, we combined our subcellular fractionation method with pulse-chase labeling and immunoprecipitation analysis. Briefly, HEK 293T cells were transfected with the HIV-1 HxBc2 provirus; 48 h later, cells were metabolically labeled with [^{35}S]methionine-cysteine for 10 min and chased for various time intervals prior to cell lysis and subcellular fractionation by Optiprep gradient centrifugation. Gag-related products in Optiprep fractions were detected by immunoprecipitation using a monoclonal anti-p24 antibody. Figure 4A and D clearly show that after 10 min of labeling (time zero h), Gag and its cleavage products were primarily detected in fractions associated with PM markers and to a lesser extent with fractions enriched with LE/MVB markers (fractions 1 to 6 and 13 and 14, respectively), suggesting that some Gag was concomitantly targeted to the PM and LE/MVB. Even though more Gag cleavage products were detected in PM-associated fractions at zero h (Fig. 4A), the kinetics of $Pr55^{gag}$ processing, calculated as the decrease of $Pr55^{gag}$ signal over time, were identical between PM- and LE/MVB-enriched fractions (Fig. 4C), suggesting that the subcellular compartment where Gag accumulates does not appear to influence its processing.

Interestingly, we observed that different processed forms of Gag were present in fractions associated with different subcellular compartments (PM versus LE/MVB). Indeed, CA-p2 (p25) was primarily detected in PM-enriched fractions, probably reflecting the fact that p24 is constantly being lost from PM-enriched fractions as virions (which contain predominantly fully processed p24 [Fig. 4B]), whereas a marked accumulation of the fully processed CA (p24) form of Gag was principally found in fractions associated to LE/MVB markers at the bottom of the gradient (Fig. 4A). Throughout the 5 h of chase, a progressive decrease of PM-associated Gag and Gag cleavage products was observed and correlated with the progressive increase of progeny virus released extracellularly, as shown by the levels of mature p24 detected in the supernatant (Fig. 4B and D). In contrast, Gag cleavage products accumulated in high-density fractions over the 5 h of chase (Fig. 4A and D), thus suggesting that virus-containing LE/MVB were not efficiently transported towards the PM, at least under our experimental conditions in HEK 293T cells. In support of this observation, we found that treatment of HIV-1-producing HEK 293T cells with nocodazole, a drug that induces microtubule depolymerization (Fig. 5A) and interferes with late endosome motility (2, 5), did not affect Gag trafficking to PM-enriched fractions (Fig. 5B), in agreement with a recent report that showed that nocodazole-induced microtubule depolymerization did not modify PM-associated Gag localization or particle release (24).

Importantly, by 2 h of chase we started detecting an important accumulation of mature Gag (p24) products in high-density fractions (Fig. 4A) that was unlikely to result from $Pr55^{gag}$ processing in these fractions (compare $Pr55^{gag}$ and $p41^{gag}$ processing over time in fractions 13 and 14). Rather, it appeared to reflect internalization of mature and/or assembling viral particles from the PM towards LE/MVB. In fact, after 2 h of chase, the subcellular location of Gag and its cleavage products was very similar to that observed at steady state (compare Fig. 2A and Fig. 4A at time 2 h), with more CA-p2 (p25) in PM-enriched fractions compared to a clear accumulation of CA (p24) in LE/MVB-enriched fractions. Importantly, similar results were obtained with polyclonal anti-p24 antibodies as well as under conditions in which proteins were denatured by boiling before immunoprecipitation as described previously (41), thus indicating that the detection method was not biased towards some Gag species or Gag-assembling structures because of lack of access to antigenic epitopes (data not shown). Finally, membrane flotation analysis indicated that 10 min of pulse-labeling was sufficient to obtain the majority (more than 60%) of Gag products associated with membranes; this association increased to almost 80% after 2 h of chase (data not shown).

Overall, these results suggest that newly synthesized Gag is primarily targeted to the PM, where assembly and release occur; a significant fraction of the remaining PM-associated Gag products appears to be subsequently internalized towards LE/MVB, where it accumulates, thus accounting for the majority of LE/MVB-associated Gag products detected at steady state.

Effect of endocytosis inhibitors on HIV-1 Gag trafficking. To confirm that the accumulation of mature Gag products in high-density fractions detected at 2 h reflected an endocytosis process from the PM towards LE/MVB, we thought to block two main routes of endocytosis. First, we used chlorpromazine, a drug known to prevent clathrin-coated pit formation at the PM (60). Even though chlorpromazine efficiently blocked clathrin-dependent endocytosis but not caveola-dependent internalization, as measured by Tfr and ChTxβ uptake (Fig. 6A and B, respectively), the accumulation of mature Gag products in high-density fractions at 2 h of chase was not affected (Fig. 6C). Indeed, quantification of the relative amounts of $Pr55^{gag}$ at zero h or quantification of mature Gag products (p25/p24) detected in PM- and LE/MVB-associated fractions at 2 h remained identical to those obtained in untreated cells (Fig. 6D

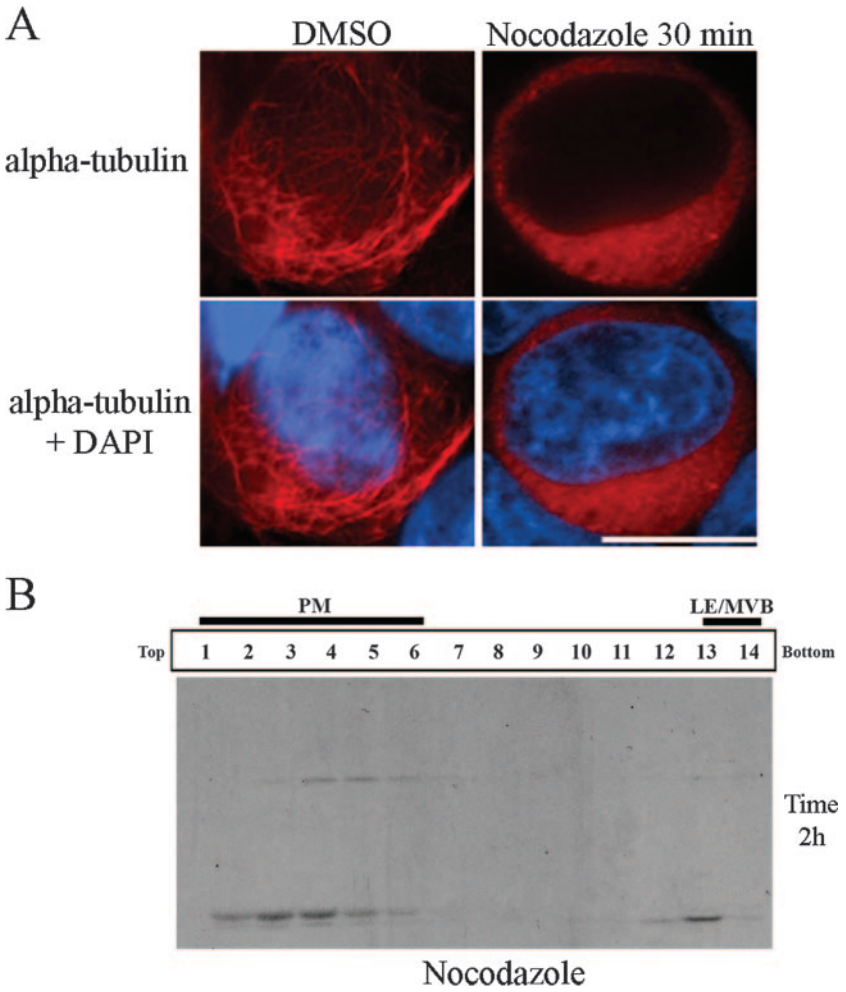

FIG. 5. Microtubule depolymerization does not affect HIV-1 Gag targeting to PM-enriched fractions. HEK 293T cells were transfected with the HxBc2 provirus. Two days after transfection, cells were incubated with nocodazole (10 μg/ml) for 30 min before being processed for immunofluorescence with an anti-α-tubulin (A). In parallel, cells were pretreated with nocodazole (10 μg/ml) for 30 min before being metabolically labeled with [^{35}S]Met-Cys for 10 min and chased for 2 h in presence of the drug. Cell lysis and subcellular fractionation were performed as described in Materials and Methods. Fourteen fractions were collected from the top of the gradient, and Gag-related products in each fraction were detected by immunoprecipitation using a monoclonal anti-p24 Ab (B). DMSO, dimethyl sulfoxide; DAPI, 4′,6′-diamidino-2-phenylindole. The data shown are representative of two independent experiments.

and E), thus suggesting that Gag internalization from PM might be clathrin independent in HEK 293T cells.

Since clathrin lattices seemed not to be required for Gag internalization, we blocked another major route of endocytosis by using sterol-binding drugs such as filipin and MβCD. These drugs interfere with caveola- or raft-dependent endocytosis by sequestering (filipin) or depleting (MβCD) cholesterol, an essential component of caveolae and lipid rafts (35, 43, 50). Filipin and MβCD efficiently blocked the uptake of ChTxβ, which was previously shown to be internalized by a cholesterol-dependent process (25) (Fig. 7B). Surprisingly, in addition to blocking ChTxβ internalization, filipin efficiently blocked Tfr uptake under our experimental conditions (Fig. 7A). Although it is very commonly reported that cholesterol is required only for cholesterol-dependent uptake mechanisms such as caveolae and lipid raft-mediated endocytosis, there is evidence for cholesterol requirement also in clathrin-mediated endocytosis (56). Interestingly, under these conditions in which clathrin and caveola/raft-dependent endocytosis were affected, we detected a significant decrease of Gag product internalization to LE/MVB-enriched fractions (Fig. 7C). Indeed, accumulation of p25/p24 Gag products in these fractions was reduced from 40% to 14%, as calculated by quantifying the relative amounts of mature Gag products detected in PM- and LE/MVB-associated fractions after 2 h of chase in control- and filipin-treated cells (Fig. 7F). Furthermore, MβCD treatment also significantly decreased mature Gag product accumulation in LE/MVB-enriched fractions at 2 h of chase (Fig. 7D); the decrease was similar to that obtained after filipin treatment, going from 40% to 19% (Fig. 7F). Importantly, removal of MβCD during the 2-h chase period partially restored mature Gag product accumulation in the LE/MVB-enriched fraction, thus indicating that the effect of cholesterol depletion was specific and reversible (data not shown). Finally, in contrast to filipin, MβCD did not affect Tfr uptake (Fig. 7A), thus suggesting that clathrin-dependent endocytosis appeared not to be involved in

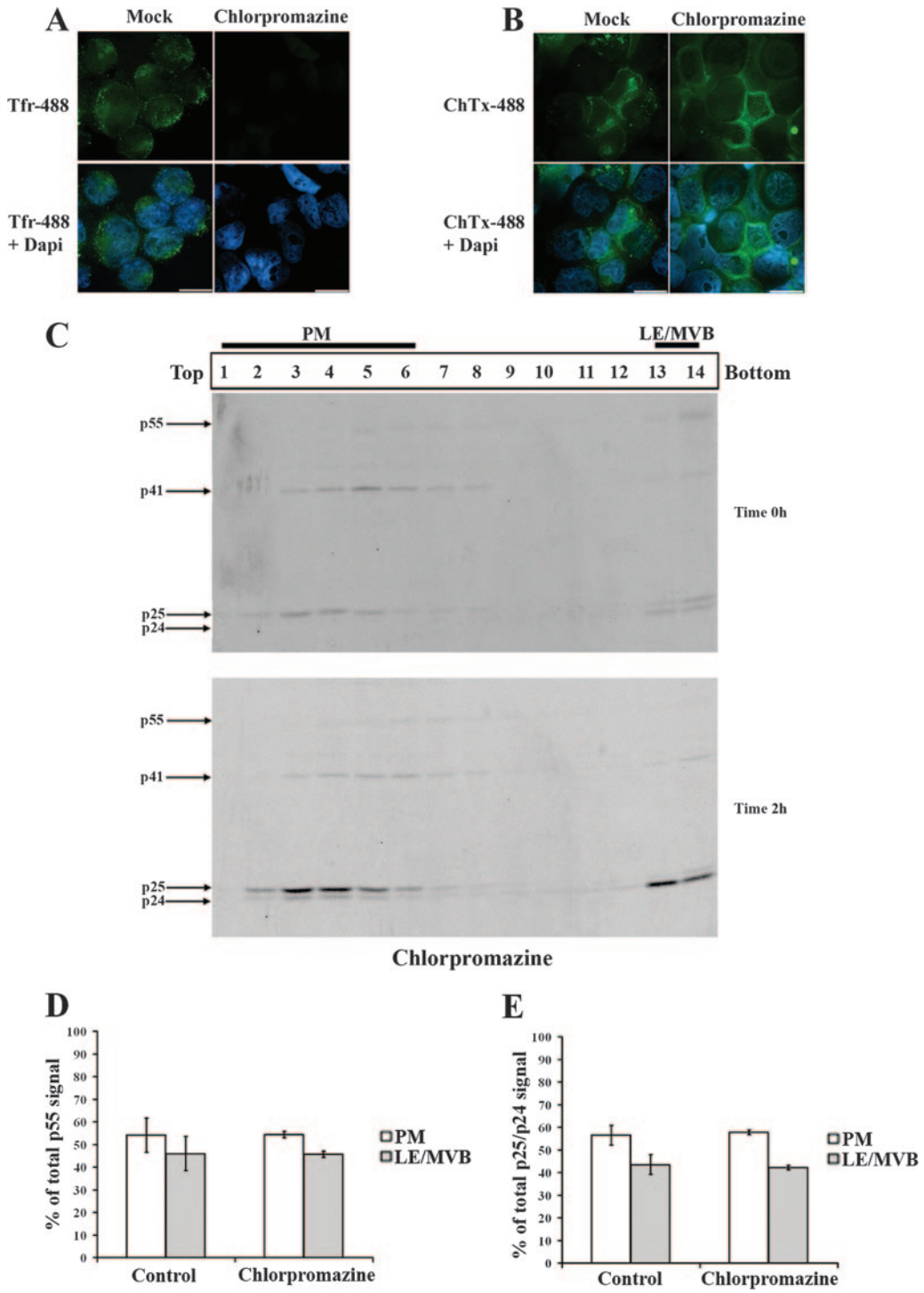

FIG. 6. Chlorpromazine, an inhibitor of clathrin-dependent endocytosis, does not affect HIV-1 Gag trafficking in HEK 293T cells. HEK 293T cells were transfected with the HxBc2 provirus. Two days after transfection, cells were pretreated with chlorpromazine (10 μg/ml) for 30 min before incubation for another 30 min at 0°C with (A) Tfr- or (B) ChTxβ–Alexa-488 conjugates. Tfr or ChTxβ internalization was allowed for 10 min at 37°C. Chlorpromazine was maintained throughout the experiment before samples were analyzed by immunofluorescence microscopy (bar, 10 μm) as described in Materials and Methods. Data shown are representative of two independent experiments. (C) In parallel, cells were metabolically labeled with [^{35}S]Met-Cys for 10 min and chased for 2 h in the presence of chlorpromazine prior to cell lysis and subcellular fractionation by Optiprep gradient centrifugation. Gag-related products in Optiprep fractions were detected by immunoprecipitation using a monoclonal anti-p24 Ab for each collected fraction. (D) Quantification of the relative amount of Pr55^{gag} detected in PM- and LE/MVB-associated fractions (1 to 6 and 13 and 14, respectively) at time zero h of chase. (E) Quantification of the relative amounts of mature Gag products (p25/p24) detected in PM or LE/MVB-associated fractions at time 2 h of chase. Gag-related signals were quantified using a PhosphorImager equipped with ImageQuant software 5.0. The data shown are means ± standard deviations of the results of five or two independent experiments: for control or chlorpromazine-treated cells, respectively.

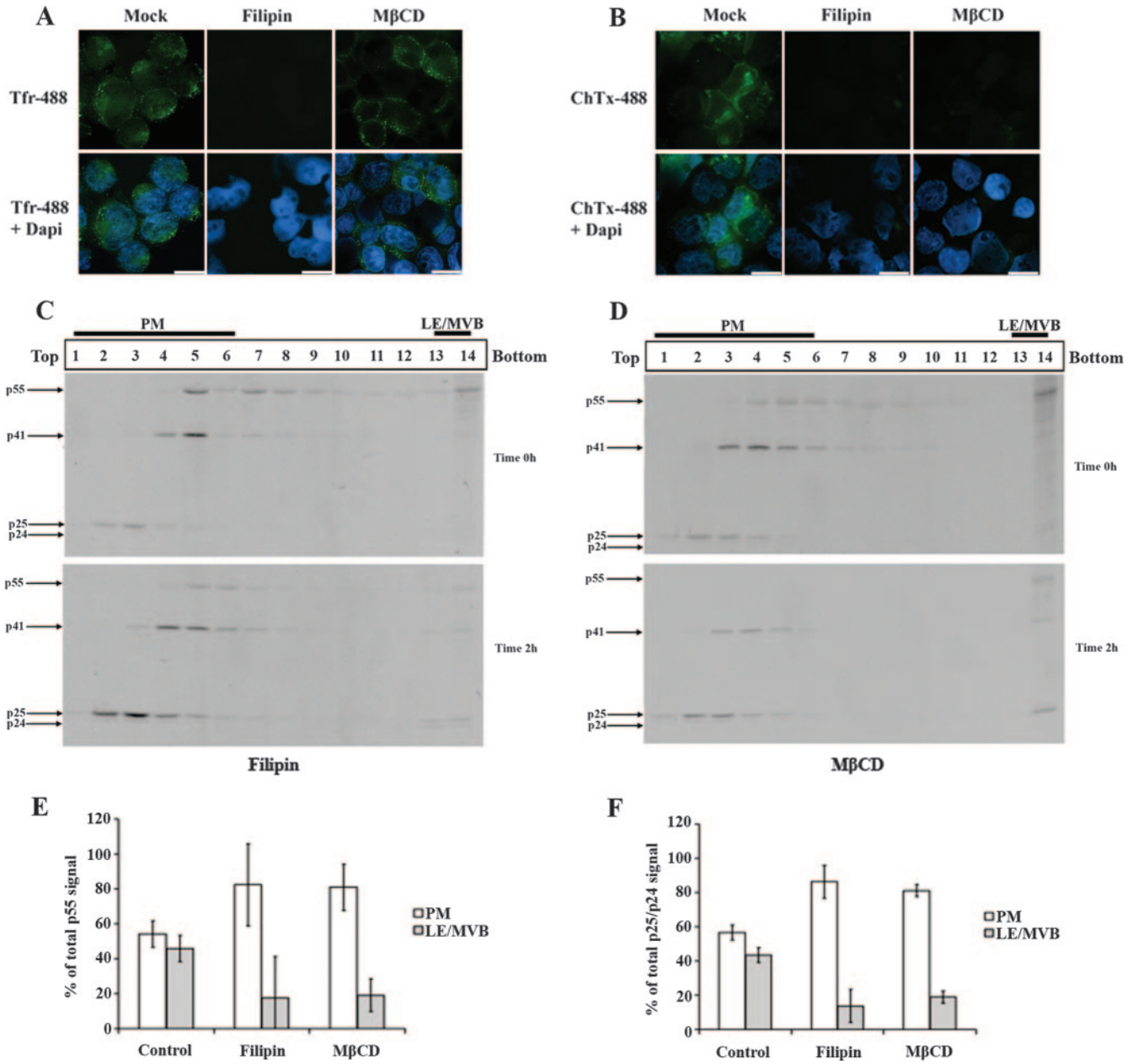

FIG. 7. Effect of cholesterol-binding drugs on HIV-1 Gag trafficking in HEK 293T cells. HEK 293T cells were transfected with the HxBc2 provirus. Two days after transfection, cells were pretreated with filipin (4 μg/ml) or MβCD (8 mM) for 30 min before incubation for another 30 min at 0°C with (A) Tfr- or (B) ChTxβ–Alexa-488 conjugates. Tfr or ChTxβ internalization was allowed for 10 min at 37°C. Endocytosis inhibitors were maintained throughout the experiment. Samples were subsequently analyzed by immunofluorescence microscopy (bar, 10 μm) as described in Materials and Methods. Data shown are representative of two independent experiments. In parallel, cells were metabolically labeled with [^{35}S]Met-Cys for 10 min and chased for 2 h in the presence of (C) filipin or (D) MβCD prior to cell lysis and subcellular fractionation by Optiprep gradient centrifugation. Gag-related products in Optiprep fractions were detected by immunoprecipitation using a monoclonal anti-p24 Ab for each collected fraction. (E) Quantification of the relative amounts of Pr55^{gag} detected in PM- and LE/MVB-associated fractions (1 to 6 and 13 and 14, respectively) at zero h of chase. (F) Quantification of the relative amounts of mature Gag products (p25/p24) detected in PM- or MVB-associated fractions at 2 h of chase. Gag-related signals were quantified as described in the legend to Fig. 6. Data shown are means ± standard deviations of the results of five control, three filipin, and two MβCD independent experiments.

Gag-related product internalization from PM to LE/MVB. Of note, filipin and MβCD treatment did not affect normal cellular mechanisms such as the processing and exocytosis of PCSK9, a proprotein convertase that is extracellularly released by the constitutive secretory pathway (data not shown), thus indicating that the effect of sterol-binding drugs on mature Gag product accumulation within LE/MVB-enriched fractions was not due to cellular toxicity.

Moreover, filipin and MβCD treatment reduced significantly the Pr55^{gag} signal detected in high-density fractions at zero h

(Fig. 7C and D, upper panels). Indeed, total $Pr55^{gag}$ signal decreased from 44% to 15% in LE/MVB-associated fractions (Fig. 7E), thus arguing also for a rapid internalization of $Pr55^{gag}$ from the PM to LE/MVB. Nonetheless, the residual $Pr55^{gag}$ detected in high-density fractions of filipin- or MβCD-treated cells and the fact that targeting of $Pr55^{gag}$ was detected in LE/MVB-associated fractions under conditions in which the labeling period was decreased to only 5 min (data not shown) suggest a possible but minor direct targeting of Gag precursor to LE/MVB. Finally, we found that chlorpromazine or sterol-binding drug treatment did not reduce Gag's ability to associate with membranes at zero h or after 2 h of chase, when the internalization process was at its peak (data not shown), suggesting that the potent reduction of Gag internalization induced by sterol-binding drugs might result from their inhibition of cholesterol-dependent uptake mechanisms. Taken together, these results suggest that the majority of newly synthesized Gag is primarily targeted to the PM; some newly synthesized Gag might be directly targeted to LE/MVB but represent a minor fraction of total Gag. Furthermore, the majority of mature Gag products present in LE/MVB after 2 h of chase result from an internalization process that is cholesterol dependent.

DISCUSSION

The precise subcellular membrane site where HIV-1 assembly is initiated has recently been the subject of intense debates. While some studies indicate that internal endosomal compartments, notably LE/MVB, represent early intermediates where Gag is first targeted prior to budding at the PM (12, 21, 30, 39, 45, 46, 48, 49, 54), more recent studies support a model in which Gag-mediated assembly mainly occurs at the PM with accumulation of Gag and viral particles in LE/MVB resulting from an internalization process from the cell surface (22, 24, 34, 51). One aspect that has complicated interpretation of the data is that, initially, most studies evaluated Gag localization at steady state by electron or fluorescence microscopy (12, 30, 38, 39, 45, 48, 54); the observation that Gag or viral particles accumulated in LE/MVB did not absolutely mean that the precursor was first targeted or assembled at this location nor did it provide any information about the route that Gag follows before reaching its steady-state subcellular destination. Furthermore, several studies analyzed Gag localization or trafficking using codon-optimized Rev-independent Gag constructs (12, 30, 38, 46, 51, 54) and/or Gag constructs encoding Gag proteins that were C-terminally fused to different tags (enhanced green fluorescent protein, enhanced cyan fluorescent protein, and tetracysteine) (12, 24, 30, 34, 38, 46, 51, 54). However, several lines of evidence suggest that the trafficking and subcellular localization of C-terminally tagged Gag molecules or Gag expressed from mRNA that do not engage the physiological Rev-dependent viral RNA nuclear export pathway may differ from those of native Gag expressed from a provirus. In that regard, it was recently reported that the mere fact of changing the length of a linker sequence between Gag and a carboxy-terminal tetracysteine tag drastically modified the localization of Gag from the PM to intracellular compartments (51). Furthermore, the presence of a carboxy-terminal hemagglutinin tag was sufficient to inhibit the endocytosis of PM-associated $Pr55^{gag}$ (22). Moreover, it was reported that introduction of mutations that did not alter Gag amino acid sequence but modified its mRNA export pathway (passing from Rev dependent to constitutive transport element [CTE] dependent) affected its steady-state localization (3, 57). In order to analyze the trafficking of native Gag molecules in the context of HIV-1-producing cells, we adapted a subcellular fractionation procedure that efficiently separates PM from LE/MVB and analyzed quantitatively the movement of Gag over time using pulse-chase labeling analysis. Importantly, these studies were performed in HEK 293T cells, an immortalized cell line that displays Gag steady-state localization at the PM and LE/MVB and that was indeed used in some studies from which arose the concept that HIV-1 assembly may be initiated in late endosomes (12, 20, 54).

One critical component of our analysis was efficient separation of PM from LE/MVB. Several lines of evidence suggest that the subcellular fractionation method that we have adapted does indeed do that. First, biochemical analysis of PM- and LE/MVB-associated markers revealed that they segregated in different fractions (Fig. 1A and B). Second, EM analysis of gradient fractions revealed an enrichment of structures that are reminiscent of PM or LE/MVB in distinct fractions (Fig. 1C); importantly, these subcellular structures were found to be associated with HIV-1 Gag products since they were specifically immunostained with anti-p24 antibodies (Fig. 3). Third, expression of HLA-DR, which is reported to induce a two- to threefold Gag relocation from PM to LE/MVB as evaluated by fluorescence microscopy (14), led to a similar increase of mature Gag product accumulation in LE/MVB-enriched fractions (Fig. 2). Furthermore, our separation method was also able to detect Vpu-mediated modulation of Gag accumulation in LE/MVB-associated fractions in HEK 293T cells cultured under confluent growth conditions (10; data not shown), in agreement with previous studies that reported increased Gag accumulation into intracellular compartments in the absence of Vpu (22, 34). Altogether, these results indicated that this subcellular fractionation method was sensitive enough to detect changes in the steady-state cellular location of Gag at the level of a whole population of HIV-1-producing cells.

By combining this subcellular fractionation procedure with short pulse-chase labeling analysis, we provide here strong evidence indicating that the majority of newly synthesized Gag is primarily targeted to the PM, where most of the productive viral particle assembly occurred. Only a minor fraction of newly synthesized $Pr55^{gag}$ was apparently directly targeted to LE/MVB (Fig. 4 and 7). In agreement with recent reports (22, 24, 34), we found that over time a significant proportion of cell surface-associated Gag products were subsequently internalized from the PM to late endosomal compartments, thus accounting for the majority of LE/MVB-associated Gag and viral particles that were previously observed at steady state using fluorescence microscopy and EM analysis. The internalization of Gag products from the PM towards LE/MVB appeared to occur very quickly after the 10 min of metabolic labeling and peaked after 2 h of chase (Fig. 4 and 7), thus underlining the need to use very short labeling periods to follow dynamically newly synthesized Gag trafficking.

Our data indicate that endocytosis of PM-associated Gag products in HEK 293T cells is sensitive to sterol-binding drugs.

Sequestration or depletion of cell surface cholesterol by treatment with filipin or MβCD, respectively, was found to drastically reduce endocytosis of Gag products (Fig. 7). These sterol-binding drugs have been previously used to inhibit endocytosis via caveolae selectively (55), thus raising the possibility that PM-associated Gag products are internalized to LE/MVB, at least in HEK 293 T cells, by a cholesterol-dependent uptake mechanism that involves caveolae or more generally lipid rafts. Cholesterol is a critical component of lipid rafts involved in caveola formation (8). When cholesterol is sequestered or extracted from the PM, lipid rafts are disrupted. A large number of studies have implicated cholesterol and sphingolipid-enriched membrane rafts in HIV-1 particle formation, production, and infectivity (29, 31, 37, 40). Furthermore, cholesterol depletion was recently reported to decrease the mobility of Gag in living cells, a process that is likely to play a major role in promoting intramolecular interactions necessary for viral assembly and release (17). Indeed, as previously reported by other studies (40), we observed that depletion of PM-associated cholesterol decreased viral release efficiency by 50 to 60% (data not shown). Given the important role of cholesterol-enriched membrane microdomains in viral particle assembly and release, we cannot entirely rule out that the effect of sterol-binding drugs on Gag internalization may be indirect rather than direct, especially if the endosomal accumulation of Gag results from internalization of fully assembled virions tethered at the cell surface, as recently suggested by Neil and coworkers (34). In contrast to sterol-binding drugs, chlorpromazine, a drug that affects clathrin-mediated endocytosis, did not have any effect on PM-associated Gag product internalization to LE/MVB (Fig. 6). These results differ from those reported by Jouvenet and colleagues (24), which indicated that Gag internalization from the PM involved clathrin-mediated endocytosis. Indeed, under their experimental conditions, expression of transdominant-negative forms of EPS 15, which inhibits clathrin-mediated endocytosis, reduced endosomal accumulation of Gag-green fluorescent protein fusion proteins. This discrepancy is perhaps related to the form of Gag (tagged Gag versus native Gag) being analyzed and/or the expression context that is used (codon-optimized Gag expressor versus proviral construct). Interestingly, recent data from Suomalainen and colleagues that are based on a fractionation procedure reveal that internalization of unprocessed $Pr55^{gag}$ expressed from a proviral construct is cholesterol dependent (inhibited by filipin) but not affected by small interfering RNA-mediated silencing of the clathrin heavy chain (M. Suomalainen, personal communication). Nevertheless, in a physiological context the mechanism and rate of internalization of Gag and viral particles from the PM are likely to be dictated in a large part by the predominant mechanism of PM internalization, which essentially occurs in all cell types via endocytic or phagocytic mechanisms. These mechanisms of internalization will vary with cell types, as indeed was recently shown with primary macrophages; in this cell type, Gag was also found to first accumulate and assemble at the PM, but a proportion appeared to be subsequently internalized by a phagocytic process (24).

Finally, under our experimental conditions we were unable to detect movement of Gag-containing LE/MVB to the PM (Fig. 4 and 5). These findings are in agreement with a recent report that found that pharmacological inhibitors (nocodazole and U18666A) that arrest late endosomal motility have no effect on accumulation of Gag at the PM or on extracellular particle release. Furthermore, the same study did not detect any viral release when viral assembly was rationally targeted to late endosomes (24). While these findings suggest that HIV particles accumulating in LE/MVB do not significantly contribute to the overall virus released extracellularly from HEK 293T cells, they do not preclude that in other cell types such as macrophages or dendritic cells and under some physiological stimulus (e.g., antigen presentation or calcium influx, which induce endosome fusion with the cell surface), virus internalized in LE/MVB is eventually released in the extracellular milieu or transmitted upon contact between cells during formation of an immunological synapse. Indeed, it was previously reported that virus accumulating intracellularly in macrophages remains infectious (26, 52) and can efficiently be transmitted to T cells for extended periods of time (52). More recently, under conditions mimicking antigen recognition by interacting T cells, dendritic cells were shown to transmit captured virions from internal compartments. However, this so-called process of *trans*-infection was limited to few captured virions and did not appear to be the predominant mode of transmission (6). Clearly, more studies are needed to better understand the role of virus accumulation in internal endosomal compartments, especially in physiological relevant cells and conditions.

Overall, the results presented herein are difficult to reconcile with data supporting a model in which HIV-1 Gag targets LE/MVB prior to budding at PM. Rather, our findings suggest that the majority of Gag is first targeted to the PM, where productive assembly occurs. Accumulation of Gag and viral particles in LE/MVB is largely the result of endocytosis of Gag from the cell surface. Importantly, Gag and virus internalized in LE/MVB are not constitutively transported to the PM to be released in the extracellular milieu. These results imply that the overall steady-state cellular localization of Gag and viral particles in different cell types will indeed be governed by the rate by which HIV particles are assembled and released at the cell surface as well as by the inherent ability of different cell types to internalize membrane from the cell surface.

ACKNOWLEDGMENTS

We thank Nabil Seidah for helpful discussion and A. Vallée for expert technical assistance with EM analysis. The polyclonal anti-p24 Ab was obtained through the NIH AIDS Research Reference and Reagent Program.

A.F. and A.O. are recipients of studentships from the Canadian Institute of Health Research (CIHR) Strategic Training Program in Cancer Research (IRCM) and the IRCM Foundation, respectively. E.A.C. is the recipient of the Canada Research Chair in Human Retrovirology. This work was supported by grants from CIHR and the Fonds de la Recherche en Santé du Québec to E.A.C.

REFERENCES

1. **Abedinpour, P., and B. Jergil.** 2003. Isolation of a caveolae-enriched fraction from rat lung by affinity partitioning and sucrose gradient centrifugation. Anal. Biochem. **313:**1–8.
2. **Aniento, F., N. Emans, G. Griffiths, and J. Gruenberg.** 1993. Cytoplasmic dynein-dependent vesicular transport from early to late endosomes. J. Cell Biol. **123:**1373–1387.
3. **Beriault, V., J. F. Clement, K. Levesque, C. Lebel, X. Yong, B. Chabot, E. A. Cohen, A. W. Cochrane, W. F. Rigby, and A. J. Mouland.** 2004. A late role for the association of hnRNP A2 with the HIV-1 hnRNP A2 response

elements in genomic RNA, Gag, and Vpr localization. J. Biol. Chem. **279:** 44141–44153.
4. **Bieniasz, P. D.** 2006. Late budding domains and host proteins in enveloped virus release. Virology **344:**55–63.
5. **Bomsel, M., R. Parton, S. A. Kuznetsov, T. A. Schroer, and J. Gruenberg.** 1990. Microtubule- and motor-dependent fusion in vitro between apical and basolateral endocytic vesicles from MDCK cells. Cell **62:**719–731.
6. **Cavrois, M., J. Neidleman, J. F. Kreisberg, and W. C. Greene.** 2007. In vitro derived dendritic cells trans-infect CD4 T cells primarily with surface-bound HIV-1 virions. PLoS Pathog. **3:**e4.
7. **Cohen, E. A., E. F. Terwilliger, Y. Jalinoos, J. Proulx, J. G. Sodroski, and W. A. Haseltine.** 1990. Identification of HIV-1 vpr product and function. J. Acquir. Immune Defic. Syndr. **3:**11–18.
8. **Crane, J. M., and L. K. Tamm.** 2004. Role of cholesterol in the formation and nature of lipid rafts in planar and spherical model membranes. Biophys. J. **86:**2965–2979.
9. **Demirov, D. G., and E. O. Freed.** 2004. Retrovirus budding. Virus Res. **106:**87–102.
10. **Deora, A., and L. Ratner.** 2001. Viral protein U (Vpu)-mediated enhancement of human immunodeficiency virus type 1 particle release depends on the rate of cellular proliferation. J. Virol. **75:**6714–6718.
11. **Ding, L., A. Derdowski, J.-J. Wang, and P. Spearman.** 2003. Independent segregation of human immunodeficiency virus type 1 Gag protein complexes and lipid rafts. J. Virol. **77:**1916–1926.
12. **Dong, X., H. Li, A. Derdowski, L. Ding, A. Burnett, X. Chen, T. R. Peters, T. S. Dermody, E. Woodruff, J. J. Wang, and P. Spearman.** 2005. AP-3 directs the intracellular trafficking of HIV-1 Gag and plays a key role in particle assembly. Cell **120:**663–674.
13. **Dugast, M., H. Toussaint, C. Dousset, and P. Benaroch.** 2005. AP2 clathrin adaptor complex, but not AP1, controls the access of the major histocompatibility complex (MHC) class II to endosomes. J. Biol. Chem. **280:**19656–19664.
14. **Finzi, A., A. Brunet, Y. Xiao, J. Thibodeau, and É. A. Cohen.** 2006. Major histocompatibility complex class II molecules promote human immunodeficiency virus type 1 assembly and budding to late endosomal/multivesicular body compartments. J. Virol. **80:**9789–9797.
15. **Ford, A. W., and P. J. Dawson.** 1994. Effect of type of container, storage temperature and humidity on the biological activity of freeze-dried alkaline phosphatase. Biologicals **22:**191–197.
16. **Freed, E. O.** 1998. HIV-1 gag proteins: diverse functions in the virus life cycle. Virology **251:**1–15.
17. **Gomez, C. Y., and T. J. Hope.** 2006. Mobility of human immunodeficiency virus type 1 $Pr55^{Gag}$ in living cells. J. Virol. **80:**8796–8806.
18. **Gottlinger, H. G.** 2001. The HIV-1 assembly machine. AIDS **15**(Suppl. 5)**:**S13–S20.
19. **Gottlinger, H. G., J. G. Sodroski, and W. A. Haseltine.** 1989. Role of capsid precursor processing and myristoylation in morphogenesis and infectivity of human immunodeficiency virus type 1. Proc. Natl. Acad. Sci. USA **86:**5781–5785.
20. **Gould, S. J., A. M. Booth, and J. E. Hildreth.** 2003. The Trojan exosome hypothesis. Proc. Natl. Acad. Sci. USA **100:**10592–10597.
21. **Grigorov, B., F. Arcanger, P. Roingeard, J. L. Darlix, and D. Muriaux.** 2006. Assembly of infectious HIV-1 in human epithelial and T-lymphoblastic cell lines. J. Mol. Biol. **359:**848–862.
22. **Harila, K., I. Prior, M. Sjöberg, A. Salminen, J. Hinkula, and M. Suomalainen.** 2006. Vpu and Tsg101 regulate intracellular targeting of the human immunodeficiency virus type 1 core protein precursor $Pr55^{gag}$. J. Virol. **80:** 3765–3772.
23. **Janvier, K., and J. S. Bonifacino.** 2005. Role of the endocytic machinery in the sorting of lysosome-associated membrane proteins. Mol. Biol. Cell **16:** 4231–4242.
24. **Jouvenet, N., S. J. Neil, C. Bess, M. C. Johnson, C. A. Virgen, S. M. Simon, and P. D. Bieniasz.** 2006. Plasma membrane is the site of productive HIV-1 particle assembly. PLoS Biol. **4:**e435.
25. **Kirkham, M., and R. G. Parton.** 2005. Clathrin-independent endocytosis: new insights into caveolae and non-caveolar lipid raft carriers. Biochim. Biophys. Acta **1745:**273–286.
26. **Kramer, B., A. Pelchen-Matthews, M. Deneka, E. Garcia, V. Piguet, and M. Marsh.** 2005. HIV interaction with endosomes in macrophages and dendritic cells. Blood Cells Mol. Dis. **35:**136–142.
27. **Lavallee, C., and E. A. Cohen.** 1993. HIV-1 HxBc2 strain encodes a truncated vpr gene product of 78 amino acids. J. Acquir. Immune Defic. Syndr. **6:**529–530.
28. **Levesque, K., Y. S. Zhao, and E. A. Cohen.** 2003. Vpu exerts a positive effect on HIV-1 infectivity by down-modulating CD4 receptor molecules at the surface of HIV-1-producing cells. J. Biol. Chem. **278:**28346–28353.
29. **Liao, Z., D. R. Graham, and J. E. Hildreth.** 2003. Lipid rafts and HIV pathogenesis: virion-associated cholesterol is required for fusion and infection of susceptible cells. AIDS Res. Hum. Retrovir. **19:**675–687.
30. **Lindwasser, O. W., and M. D. Resh.** 2004. Human immunodeficiency virus type 1 Gag contains a dileucine-like motif that regulates association with multivesicular bodies. J. Virol. **78:**6013–6023.
31. **Lindwasser, O. W., and M. D. Resh.** 2001. Multimerization of human immunodeficiency virus type 1 Gag promotes its localization to barges, raft-like membrane microdomains. J. Virol. **75:**7913–7924.
32. **Micheva, K. D., A. Vallee, C. Beaulieu, I. M. Herman, and N. Leclerc.** 1998. beta-Actin is confined to structures having high capacity of remodelling in developing and adult rat cerebellum. Eur. J. Neurosci. **10:**3785–3798.
33. **Morita, E., and W. I. Sundquist.** 2004. Retrovirus budding. Annu. Rev. Cell Dev. Biol. **20:**395–425.
34. **Neil, S. J., S. W. Eastman, N. Jouvenet, and P. D. Bieniasz.** 2006. HIV-1 Vpu promotes release and prevents endocytosis of nascent retrovirus particles from the plasma membrane. PLoS Pathog. **2:**e39.
35. **Neufeld, E. B., A. M. Cooney, J. Pitha, E. A. Dawidowicz, N. K. Dwyer, P. G. Pentchev, and E. J. Blanchette-Mackie.** 1996. Intracellular trafficking of cholesterol monitored with a cyclodextrin. J. Biol. Chem. **271:**21604–21613.
36. **Nguyen, D. G., A. Booth, S. J. Gould, and J. E. Hildreth.** 2003. Evidence that HIV budding in primary macrophages occurs through the exosome release pathway. J. Biol. Chem. **278:**52347–52354.
37. **Nguyen, D. H., and J. E. K. Hildreth.** 2000. Evidence for budding of human immunodeficiency virus type 1 selectively from glycolipid-enriched membrane lipid rafts. J. Virol. **74:**3264–3272.
38. **Nydegger, S., M. Foti, A. Derdowski, P. Spearman, and M. Thali.** 2003. HIV-1 egress is gated through late endosomal membranes. Traffic **4:**902–910.
39. **Ono, A., and E. O. Freed.** 2004. Cell-type-dependent targeting of human immunodeficiency virus type 1 assembly to the plasma membrane and the multivesicular body. J. Virol. **78:**1552–1563.
40. **Ono, A., and E. O. Freed.** 2001. Plasma membrane rafts play a critical role in HIV-1 assembly and release. Proc. Natl. Acad. Sci. USA **98:**13925–13930.
41. **Ono, A., A. A. Waheed, A. Joshi, and E. O. Freed.** 2005. Association of human immunodeficiency virus type 1 Gag with membrane does not require highly basic sequences in the nucleocapsid: use of a novel Gag multimerization assay. J. Virol. **79:**14131–14140.
42. **Orenstein, J. M., M. S. Meltzer, T. Phipps, and H. E. Gendelman.** 1988. Cytoplasmic assembly and accumulation of human immunodeficiency virus types 1 and 2 in recombinant human colony-stimulating factor-1-treated human monocytes: an ultrastructural study. J. Virol. **62:**2578–2586.
43. **Orlandi, P. A., and P. H. Fishman.** 1998. Filipin-dependent inhibition of cholera toxin: evidence for toxin internalization and activation through caveolae-like domains. J. Cell Biol. **141:**905–915.
44. **Panina-Bordignon, P., X. T. Fu, A. Lanzavecchia, and R. W. Karr.** 1992. Identification of HLA-DR alpha chain residues critical for binding of the toxic shock syndrome toxin superantigen. J. Exp. Med. **176:**1779–1784.
45. **Pelchen-Matthews, A., B. Kramer, and M. Marsh.** 2003. Infectious HIV-1 assembles in late endosomes in primary macrophages. J. Cell Biol. **162:**443–455.
46. **Perlman, M., and M. D. Resh.** 2006. Identification of an intracellular trafficking and assembly pathway for HIV-1 gag. Traffic **7:**731–745.
47. **Radka, S. F., C. E. Machamer, and P. Cresswell.** 1984. Analysis of monoclonal antibodies reactive with human class II beta chains by two-dimensional electrophoresis and Western blotting. Hum. Immunol. **10:**177–186.
48. **Raposo, G., M. Moore, D. Innes, R. Leijendekker, A. Leigh-Brown, P. Benaroch, and H. Geuze.** 2002. Human macrophages accumulate HIV-1 particles in MHC II compartments. Traffic **3:**718–729.
49. **Resh, M. D.** 2005. Intracellular trafficking of HIV-1 Gag: how Gag interacts with cell membranes and makes viral particles. AIDS Rev. **7:**84–91.
50. **Rothberg, K. G., J. E. Heuser, W. C. Donzell, Y. S. Ying, J. R. Glenney, and R. G. Anderson.** 1992. Caveolin, a protein component of caveolae membrane coats. Cell **68:**673–682.
51. **Rudner, L., S. Nydegger, L. V. Coren, K. Nagashima, M. Thali, and D. E. Ott.** 2005. Dynamic fluorescent imaging of human immunodeficiency virus type 1 Gag in live cells by biarsenical labeling. J. Virol. **79:**4055–4065.
52. **Sharova, N., C. Swingler, M. Sharkey, and M. Stevenson.** 2005. Macrophages archive HIV-1 virions for dissemination in trans. EMBO J. **24:**2481–2489. [Epub ahead of print.]
53. **Sheff, D. R., E. A. Daro, M. Hull, and I. Mellman.** 1999. The receptor recycling pathway contains two distinct populations of early endosomes with different sorting functions. J. Cell Biol. **145:**123–139.
54. **Sherer, N. M., M. J. Lehmann, L. F. Jimenez-Soto, A. Ingmundson, S. M. Horner, G. Cicchetti, P. G. Allen, M. Pypaert, J. M. Cunningham, and W. Mothes.** 2003. Visualization of retroviral replication in living cells reveals budding into multivesicular bodies. Traffic **4:**785–801.
55. **Sieczkarski, S. B., and G. R. Whittaker.** 2002. Dissecting virus entry via endocytosis. J. Gen. Virol. **83:**1535–1545.
56. **Subtil, A., I. Gaidarov, K. Kobylarz, M. A. Lampson, J. H. Keen, and T. E. McGraw.** 1999. Acute cholesterol depletion inhibits clathrin-coated pit budding. Proc. Natl. Acad. Sci. USA **96:**6775–6780.
57. **Swanson, C. M., B. A. Puffer, K. M. Ahmad, R. W. Doms, and M. H. Malim.** 2004. Retroviral mRNA nuclear export elements regulate protein function and virion assembly. EMBO J. **23:**2632–2640.
58. **Thorn, H., K. G. Stenkula, M. Karlsson, U. Ortegren, F. H. Nystrom, J. Gustavsson, and P. Stralfors.** 2003. Cell surface orifices of caveolae and

localization of caveolin to the necks of caveolae in adipocytes. Mol. Biol. Cell **14:**3967–3976.
59. **Tritel, M., and M. D. Resh.** 2000. Kinetic analysis of human immunodeficiency virus type 1 assembly reveals the presence of sequential intermediates. J. Virol. **74:**5845–5855.
60. **Wang, L. H., K. G. Rothberg, and R. G. Anderson.** 1993. Mis-assembly of clathrin lattices on endosomes reveals a regulatory switch for coated pit formation. J. Cell Biol. **123:**1107–1117.
61. **Yao, X.-J., R. A. Subbramanian, N. Rougeau, F. Boisvert, D. Bergeron, and E. A. Cohen.** 1995. Mutagenic analysis of human immunodeficiency virus type 1 Vpr: role of a predicted N-terminal alpha-helical structure in Vpr nuclear localization and virion incorporation. J. Virol. **69:**7032–7044.